

Supporting Information

Spherical and Sheetlike Ag/AgCl Nanostructures: Interesting Photocatalysts with Unusual Facet–Dependent yet Substrate–Sensitive Reactivity

Yunfan Shen,^{†,‡} Penglei Chen,^{*,†,‡} Dan Xiao,^{†,‡} Chuncheng Chen,[†] Mingshan Zhu,[†]
Tiesheng Li,[‡] Wangong Ma,[†] and Minghua Liu[†]

[†]Beijing National Laboratory for Molecular Science, CAS Key Laboratory of Colloid, Interface, Chemical Thermodynamics, Institute of Chemistry, Chinese Academy of Sciences, No. 2 Zhongguancun Beiyijie, Beijing 100190, People's Republic of China.

[‡]College of Chemistry and Molecular Engineering, Zhengzhou University, 100 Science Road, Zhengzhou, Henan 450001, People's Republic of China.

Fax: (+) 86-10-62569564; Tel: (+) 86-10-82615803.

E-mail: chenpl@iccas.ac.cn; cpl@zzu.edu.cn

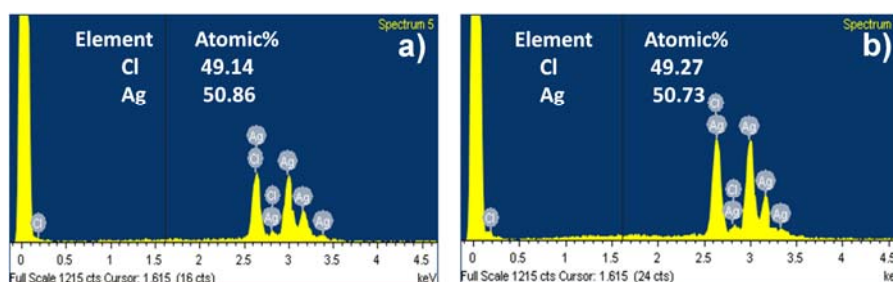


Figure S1. EDX elemental analysis of our nanospheres (a) and nanosheets (b).

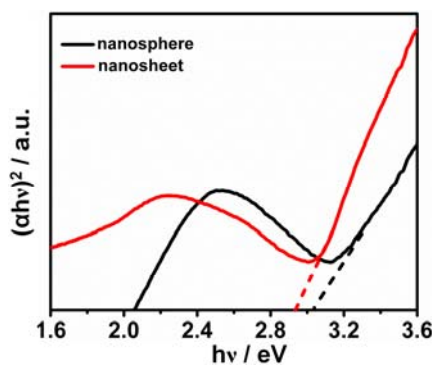


Figure S2. Plots of $(\alpha h\nu)^2$ vs. photon energy for our nanospheres (black) and nanosheets (red).

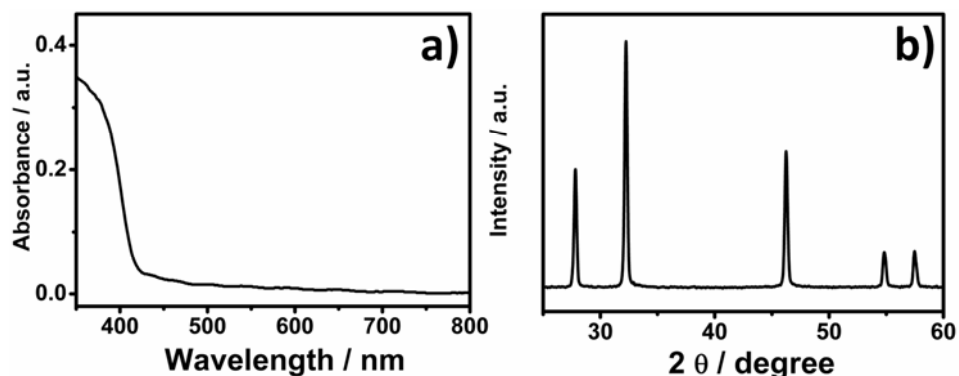


Figure S3. UV–visible diffuse reflectance spectrum (A) and PXRD pattern (B) of the AgCl species fabricated in a strictly darkened room, where there was only a weak infrared lamp on the wall.

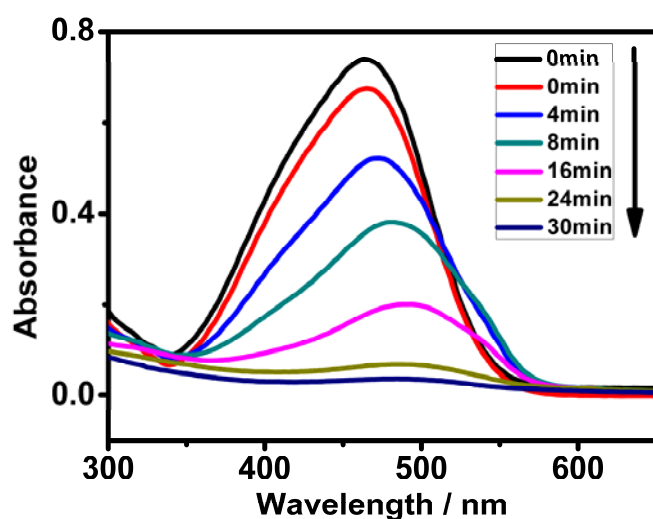


Figure S4. Typical real-time absorption spectra of MO dye during the photodegradation process over our Ag/AgCl nanosheets under visible light ($\lambda > 420$) irradiations. The black and red curves marked as 0 min are the absorption spectra detected from the original MO solution before (black) and after (red) the dark adsorption experiment, respectively.

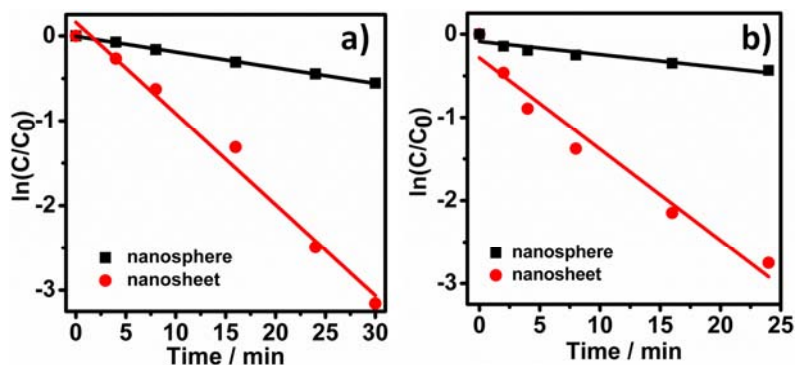


Figure S5. The kinetic linear simulation curves of our nanospheres (black) and nanosheets (red) towards the photodegradation of MO pollutant under visible (a, $\lambda > 420$) and UV (b, $\lambda = 365$ nm) light irradiations.

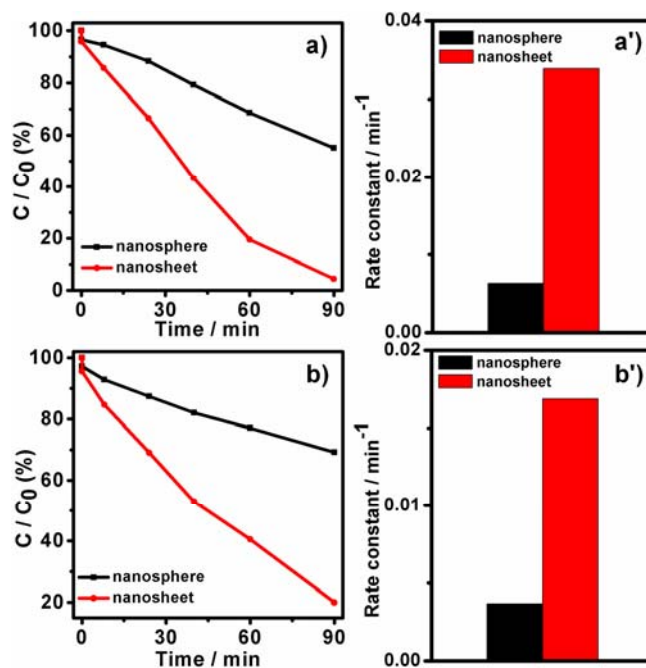


Figure S6. Photocatalytic performances (a and b) and the corresponding reaction rate constants (a' and b') for the photodegradation of MO over our nanospheres (black) and nanosheets (red). The photocatalytic experiments are carried out in combination with a bandpass filter of 500 ± 15 nm (a and a') and 550 ± 15 nm (b and b'), respectively.

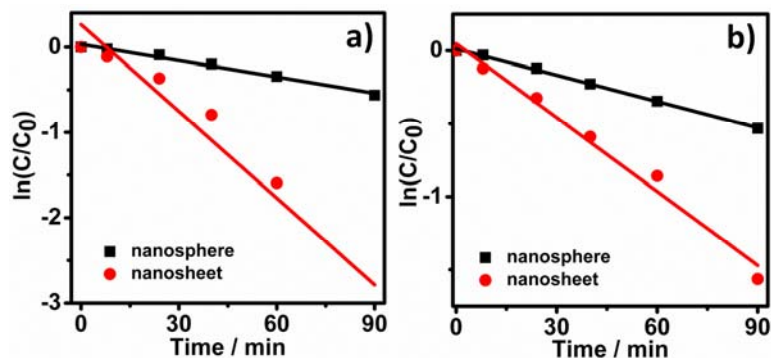


Figure S7. The kinetic linear simulation curves of our nanospheres (black) and nanosheets (red) towards the photodegradation of MO pollutant. The photocatalytic experiments are carried out in combination with a bandpass filter of 500 ± 15 nm (a) and 550 ± 15 nm (b), respectively.

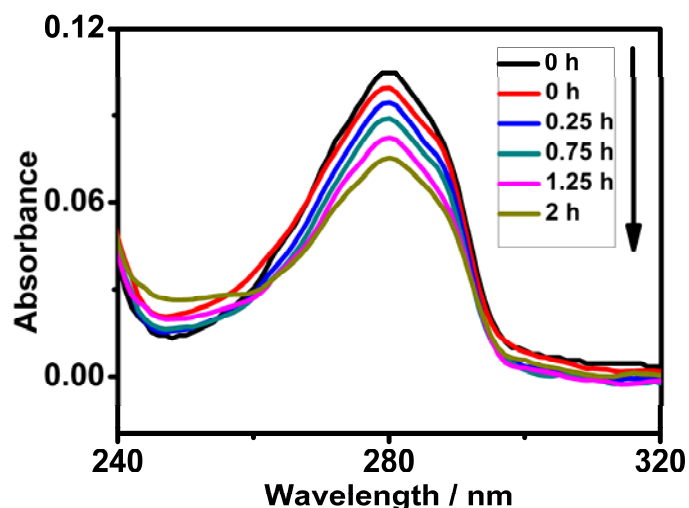


Figure S8. Typical real-time absorption spectra of 4-CP during the photodegradation process over our Ag/AgCl nanospheres. The photocatalytic experiments are carried out in combination with a bandpass filter of 550 ± 15 nm. The black and red curves marked as 0 min are the absorption spectra detected from the original MO solution before (black) and after (red) the dark adsorption experiment, respectively.

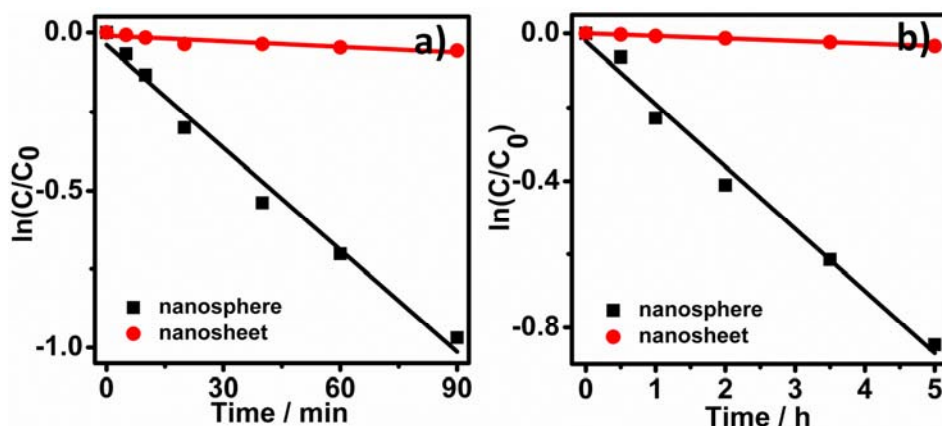


Figure S9. The kinetic linear simulation curves of our nanospheres (black) and nanosheets (red) towards the photodegradation of 4-CP under visible (a, $\lambda > 420$) and UV (b, $\lambda = 365$ nm) light irradiations.

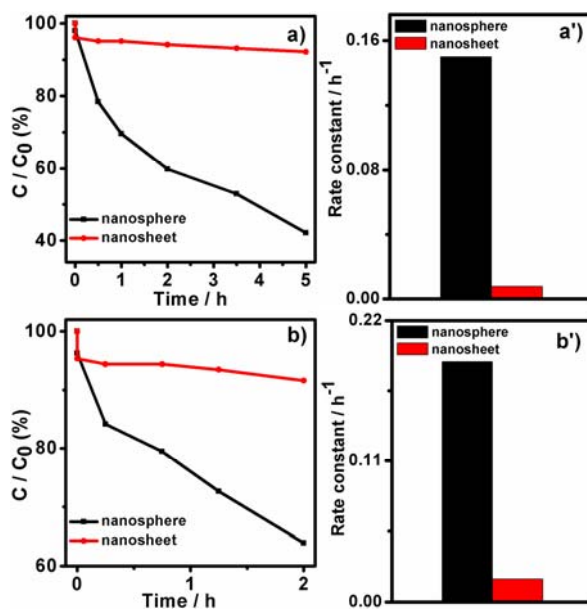


Figure S10. Photocatalytic performances (a and b) and the corresponding reaction rate constants (a' and b') for the photodegradation of 4-CP over our nanospheres (black) and nanosheets (red). The photocatalytic experiments are carried out in combination with a bandpass filter of 500 ± 15 nm (a and a') and 550 ± 15 nm (b and b'), respectively.

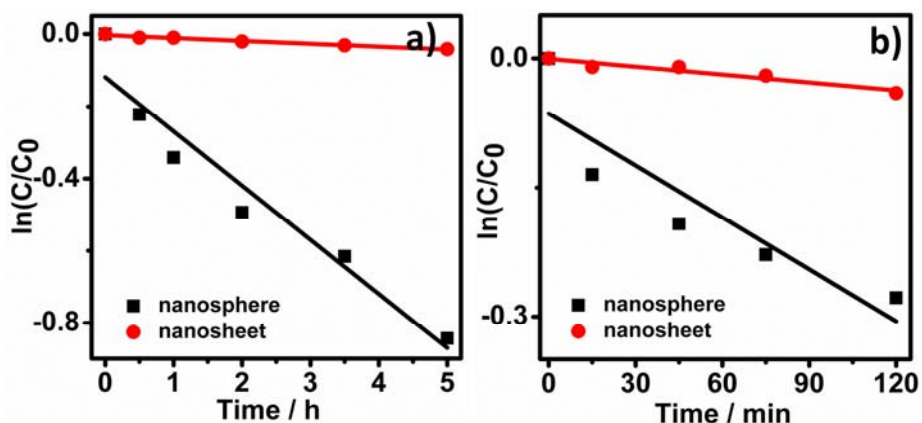


Figure S11. The kinetic linear simulation curves of our nanospheres (black) and nanosheets (red) towards the photodegradation of 4-CP. The photocatalytic experiments are carried out in combination with a bandpass filter of 500 ± 15 nm (a) and 550 ± 15 nm (b), respectively.

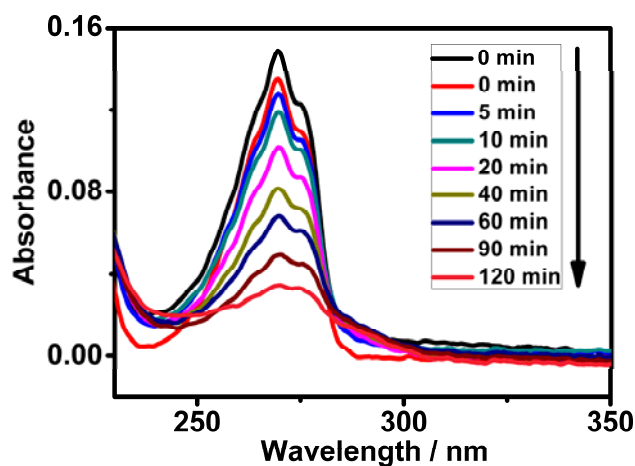


Figure S12. Typical real-time absorption spectra of phenol during the photodegradation process over our Ag/AgCl nanospheres under UV light ($\lambda = 365$ nm) irradiation. The black and red curves marked as 0 min are the absorption spectra detected from the original phenol solution before (black) and after (red) the dark adsorption experiment, respectively.

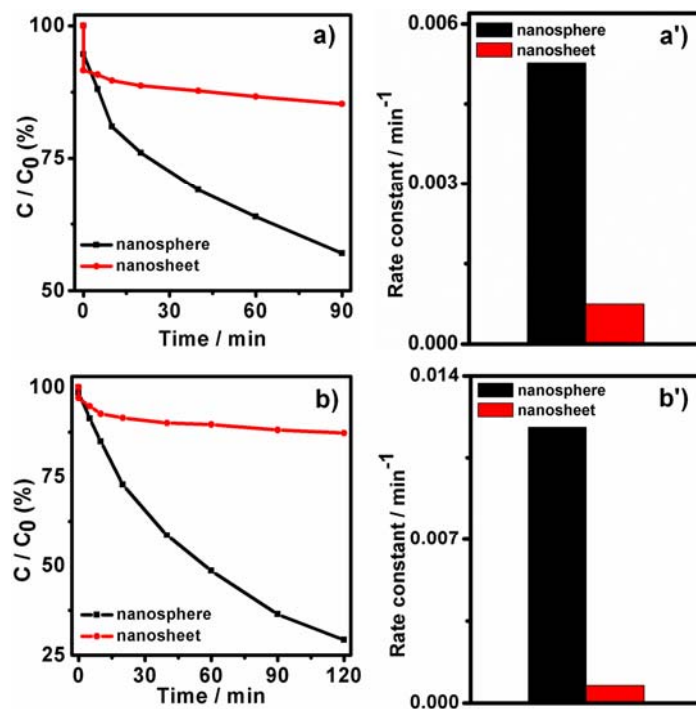


Figure S13. Photocatalytic performances (a and b) and the corresponding reaction rate constants (a' and b') for the photodegradation of phenol over our nanospheres (black) and nanosheets (red) under visible (a and a', $\lambda > 420$) and UV (b and b', $\lambda = 365$ nm) light irradiation.

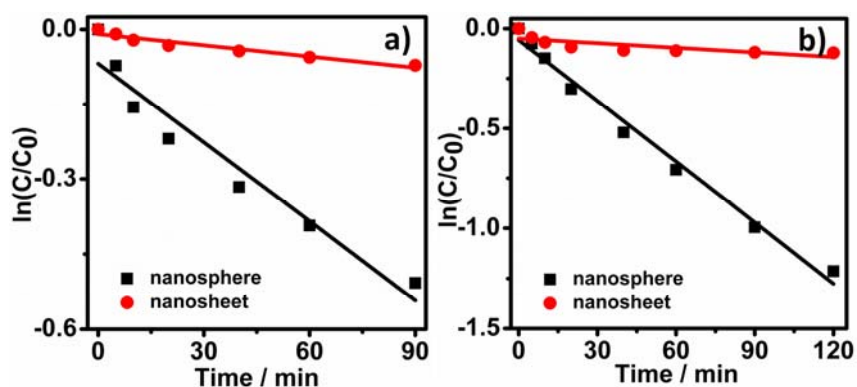


Figure S14. The kinetic linear simulation curves of our nanospheres (black) and nanosheets (red) towards the photodegradation of phenol under visible (a, $\lambda > 420$) and UV (b, $\lambda = 365$ nm) light irradiation.

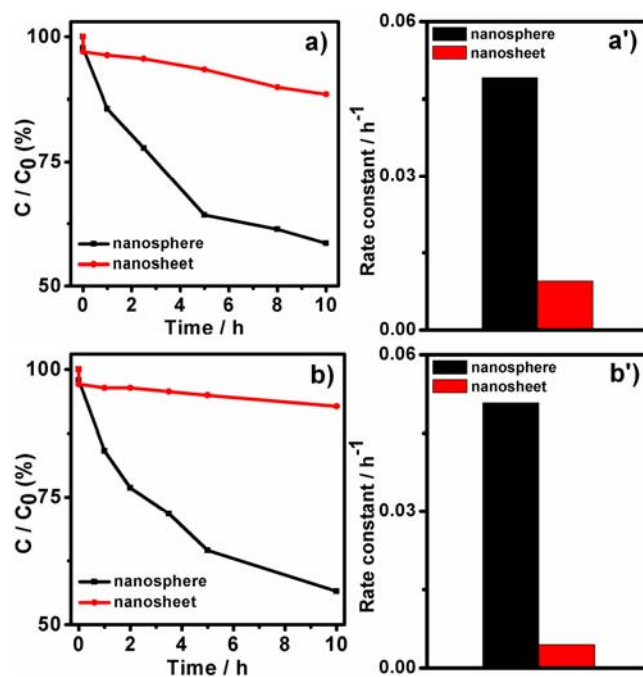


Figure 15. Photocatalytic performances (a and b) and the corresponding reaction rate constants (a' and b') for the photodegradation of phenol over our nanospheres (black) and nanosheets (red). The photocatalytic experiments are carried out in combination with a bandpass filter of 500 ± 15 nm (a and a') and 550 ± 15 nm (b and b'), respectively.

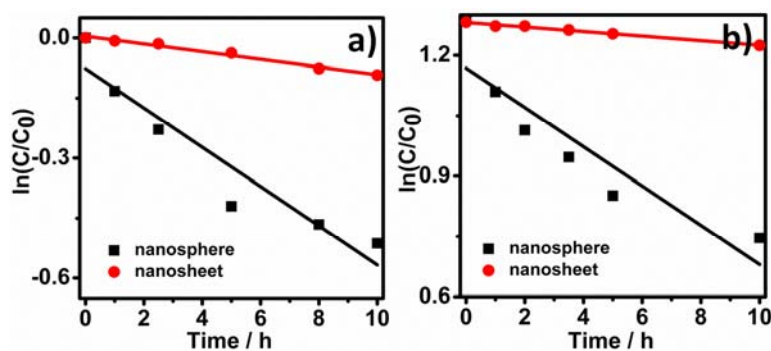


Figure 16. The kinetic linear simulation curves of our nanospheres (black) and nanosheets (red) towards the photodegradation of phenol. The photocatalytic experiments are carried out in combination with a bandpass filter of 500 ± 15 nm (a) and 550 ± 15 nm (b), respectively.

Table S1. A summary of the rate constant of MO photodegradation over our nanospheres and nanosheets driven by various lights of different wavelengths. The corresponding rate constant calibrated in terms of a correlation with regard to the extinction coefficients of the catalysts are presented in the corresponding parentheses.

| Catalyst | $\lambda = 365 \text{ nm}$ | $\lambda = 500\pm 15 \text{ nm}$ | $\lambda = 550\pm 15 \text{ nm}$ |
|------------|--|--|--|
| nanosphere | $1 \times 10^{-2} (5.6 \times 10^{-2}) \text{ min}^{-1}$ | $6.4 \times 10^{-3} (3.6 \times 10^{-2}) \text{ min}^{-1}$ | $3.7 \times 10^{-3} (2.5 \times 10^{-2}) \text{ min}^{-1}$ |
| nanosheet | $1 \times 10^{-1} (2.9 \times 10^{-1}) \text{ min}^{-1}$ | $3.4 \times 10^{-2} (2.6 \times 10^{-1}) \text{ min}^{-1}$ | $1.7 \times 10^{-2} (1.1 \times 10^{-1}) \text{ min}^{-1}$ |

Table S2. A summary of the rate constant of 4-CP photodegradation over our nanospheres and nanosheets driven by various lights of different wavelengths. The corresponding rate constant calibrated in terms of a correlation with regard to the extinction coefficients of the catalysts are presented in the corresponding parentheses.

| Catalyst | $\lambda = 365 \text{ nm}$ | $\lambda = 500\pm 15 \text{ nm}$ | $\lambda = 550\pm 15 \text{ nm}$ |
|------------|--|--|--|
| nanosphere | $1.7 \times 10^{-1} (9.4 \times 10^{-1}) \text{ h}^{-1}$ | $1.5 \times 10^{-1} (8.3 \times 10^{-1}) \text{ h}^{-1}$ | $1.9 \times 10^{-1} (1.3 \times 10^0) \text{ h}^{-1}$ |
| nanosheet | $6.8 \times 10^{-3} (2.0 \times 10^{-2}) \text{ h}^{-1}$ | $7.8 \times 10^{-3} (6.0 \times 10^{-2}) \text{ h}^{-1}$ | $1.8 \times 10^{-2} (1.1 \times 10^{-1}) \text{ h}^{-1}$ |

Table 3. A summary of the rate constant of phenol photodegradation over our nanospheres and nanosheets driven by various lights of different wavelengths. The corresponding rate constant calibrated in terms of a correlation with regard to the extinction coefficients of the catalysts are presented in the corresponding parentheses.

| Catalyst | $\lambda = 365 \text{ nm}$ | $\lambda = 500\pm 15 \text{ nm}$ | $\lambda = 550\pm 15 \text{ nm}$ |
|------------|--|--|--|
| nanosphere | $1.0 \times 10^{-2} (5.6 \times 10^{-2}) \text{ min}^{-1}$ | $4.9 \times 10^{-2} (2.7 \times 10^{-1}) \text{ h}^{-1}$ | $5.1 \times 10^{-2} (3.4 \times 10^{-1}) \text{ h}^{-1}$ |
| nanosheet | $7.7 \times 10^{-4} (2.3 \times 10^{-3}) \text{ min}^{-1}$ | $9.6 \times 10^{-3} (7.4 \times 10^{-2}) \text{ h}^{-1}$ | $4.5 \times 10^{-3} (2.8 \times 10^{-2}) \text{ h}^{-1}$ |